



From sMRI to task-fMRI: A unified geometric deep learning framework for cross-modal brain anatomo-functional mapping

Zhiyuan Zhu ^{a,b}, Taicheng Huang ^c, Zonglei Zhen ^c, Boyu Wang ^d, Xia Wu ^{a,b,*}, Shuo Li ^{e,f}

^a School of Artificial Intelligence, Beijing Normal University, Beijing, China

^b Engineering Research Center of Intelligent Technology and Educational Application (Beijing Normal University), Ministry of Education, Beijing, China

^c Faculty of Psychology, Beijing Normal University, Beijing, China

^d Department of Computer Science, Western University, ON, Canada

^e Department of Computer and Data Science, Case Western Reserve University, Ohio, USA

^f Department of Biomedical Engineering, Case Western Reserve University, Ohio, USA



ARTICLE INFO

Keywords:

sMRI
Task-fMRI
Brain anatomo-functional mapping
Geometric deep learning

ABSTRACT

Achieving predictions of brain functional activation patterns/task-fMRI maps from its underlying anatomy is an important yet challenging problem. Once successful, it will not only open up new ways to understand how brain anatomy influences functional organization of the brain, but also provide new technical support for the clinical use of anatomical information to guide the localization of cortical functional areas. However, due to the non-Euclidean complex architecture of brain anatomy and the inherent low signal-to-noise ratio (SNR) properties of fMRI signals, the key challenge in building such a cross-modal brain anatomo-functional mapping is how to effectively learn the context-aware information of brain anatomy and overcome the interference of noise-containing task-fMRI labels on the learning process. In this work, we propose a Unified Geometric Deep Learning framework (**BrainUGDL**) to perform the cross-modal brain anatomo-functional mapping task. Considering that both global and local structures of brain anatomy have an impact on brain functions from their respective perspectives, we innovatively propose the novel Global Graph Encoding (GGE) unit and Local Graph Attention (LGA) unit embedded into two parallel branches, focusing on learning the high-level global and local context information, respectively. Specifically, GGE learns the global context information of each mesh vertex by building and encoding global interactions, and LGA learns the local context information of each mesh vertex by selectively aggregating patch structure enhanced features from its spatial neighbors. The information learnt from the two branches is then fused to form a comprehensive representation of brain anatomical features for final brain function predictions. To address the inevitable measurement noise in task-fMRI labels, we further elaborate a novel uncertainty-filtered learning mechanism, which enables BrainUGDL to realize revised learning from the noise-containing labels through the estimated uncertainty. Experiments across seven open task-fMRI datasets from human connectome project (HCP) demonstrate the superiority of BrainUGDL. To our best knowledge, our proposed BrainUGDL is the first to achieve the prediction of individual task-fMRI maps solely based on brain sMRI data.

1. Introduction

Exploring brain anatomo-functional relationship has always been a core issue in neuroscience (De Benedictis et al., 2014; Amiez and Petrides, 2014; Jiang et al., 2021), which is critical for us to understand how individual behavioral differences or disease progressions emerge from the underlying brain anatomy (Schultz et al., 1994; Papo, 2019; Besson et al., 2021). Non-invasive imaging modalities of structural Magnetic Resonance Imaging (sMRI) and task-functional Magnetic Resonance Imaging (task-fMRI) provide the necessary data source for

modeling their relationships. Specifically, sMRI explicitly provides individual brain anatomical structure, and task-fMRI provides individual brain functional activation patterns/task-fMRI maps under different cognitive task contrasts (see Fig. 1).

For decades, numerous studies have shown that the alternations in brain anatomy are strongly coupled with individual differences in brain functions (Amiez and Petrides, 2014; Sun et al., 2016; Amiez and Petrides, 2018; Im and Grant, 2019), therefore, a reasonable idea is to use brain anatomy to predict brain functions. Just like the conformation

* Corresponding author.

E-mail address: wuxia@bnu.edu.cn (X. Wu).

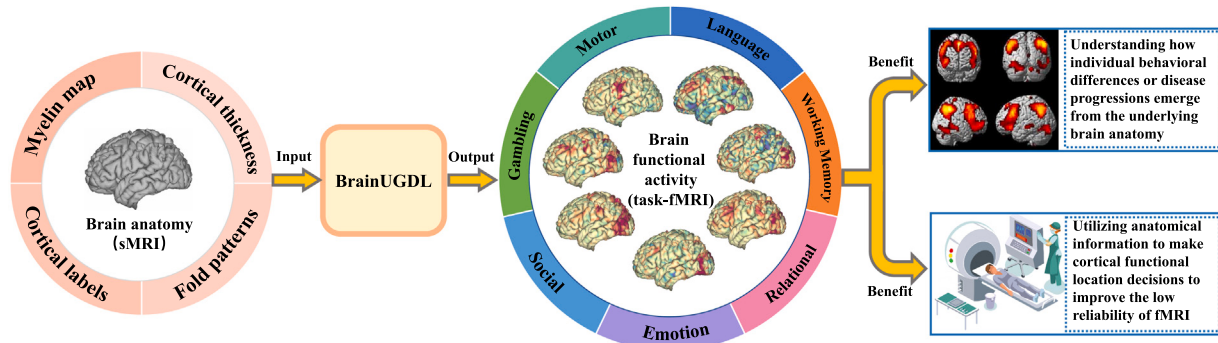


Fig. 1. Our BrainUGDL aims to predict brain functional activation patterns/task-fMRI maps under different cognitive task contrasts from individual inherent brain anatomy. Once successful, it will not only provide new ways to understand how brain functional abnormalities arise from the underlying anatomy, but will also provide new technical support for using anatomical information to guide the localization of cortical functional areas, improving the low reliability of fMRI in clinical applications.

of a protein determines its chemical properties and, ultimately, its biological function (Suárez et al., 2020), neuroscience has generally suggested that the unique folds of brain anatomy formed by the rapid expansion of the cortical mantle provide the basis for the formation of brain functions (Budday et al., 2015; Fernández et al., 2016; Calhoun, 2018; Long et al., 2018), that is, the brain anatomy should be possible, at least partially, to predict brain functions. Once successful, it will not only provide new ways to understand how brain functional abnormalities arise from the underlying anatomy (Jiang et al., 2021), but will also provide new technical support to improve the low reliability of fMRI in clinical application by using anatomical information to guide the localization of cortical functional areas (Ellis et al., 2020).

Thus, our target is to build a mapping model \mathcal{F} to achieve the prediction from brain anatomy (derived from sMRI) to brain functional activation patterns (derived from task-fMRI) at the individual level, this process can be defined as:

$$Y_{function}^i = \mathcal{F}(X_{anatomy}^i) \quad (1)$$

Unfortunately, building such a cross-modal brain anatomo-functional mapping model still faces challenges. Firstly, although modern machine learning algorithms represented by deep neural networks (Le-Cun et al., 2015) show great potential in extracting effective high-level context features, the brain anatomical surface data derived from sMRI belongs to non-Euclidean architecture (Thompson et al., 1996), which challenges most deep learning models that originally designed for Euclidean-structured data, such as convolutional neural networks (CNNs) (LeCun et al., 1995). Recently, geometric deep learning aims to fill the gap by generalizing deep learning models from a 2D Euclidean plane to a 3D non-Euclidean geometric manifold (Monti et al., 2017; Cao et al., 2020; He et al., 2020). However, studies have shown that both global and local structures of brain anatomy have an impact on brain functions from their own aspects (details in Section 2.1), the existing geometric deep learning methods have not yet established an effective global and local context-aware feature extraction mechanism, which prevents us from building reliable anatomo-functional mappings. Secondly, due to MRI system-related instabilities and physiological fluctuations (Hutton et al., 2011), the measures of task-fMRI maps generally inevitably contain noise (Biswal et al., 1996; Hutton et al., 2011). However, these noise-containing labels will largely compromise the learning process and pose another challenge for building the cross-modal brain anatomo-functional mapping model.

In this work, we propose a unified geometric deep learning framework (**BrainUGDL**), which aims to effectively learn global and local context features of the 3D brain anatomy, thereby facilitating mapping to brain functions. BrainUGDL directly takes the 3D brain anatomy as input, and output AI-predicted task-fMRI maps, making it comparable to the actual measured ones. As illustrated in Fig. 2(b), considering that both global and local features of brain anatomy have an impact on brain functions from their respective perspectives, BrainUGDL is designed

with two parallel geometric deep learning branches to focus on encoding global and local context features of brain anatomy, respectively. Specifically, in the global-context branch, we propose a novel Global Graph Encoding (GGE) unit to learn the global context of each mesh vertex by building and encoding the global interactions. In the local-context branch, a Local Graph Attention (LGA) unit is proposed, which aims to learn the local context of each vertex by selectively aggregating patch structure enhanced features from its spatial neighbors. Subsequently, the global and local context information of these two branches are fused to obtain a comprehensive representation of anatomical features for the final predictions of task-fMRI maps. In addition, to address the inevitable measurement noise in fMRI, an uncertainty-filtered learning mechanism is further proposed, which enables BrainUGDL to realize revised learning from the noise-containing task-fMRI labels through the estimated uncertainty, reducing the interference of noisy labels on the learning process.

We validate BrainUGDL across seven open task-fMRI datasets from human connectome project (HCP) (Van Essen et al., 2013). Experimental results show that BrainUGDL is not only capable of achieving such across-modal anatomo-functional predictions, but is also able to capture nuanced inter-individual differences. The excellent performance makes it promising to make clinical decisions on individual cortical functional localization using sMRI data. Generally, the main contributions of this study are summarized as follows:

- For the first time, we achieved the prediction of individual task-fMRI maps solely based on brain sMRI data. Its excellent performance on seven open task-fMRI datasets of HCP demonstrates the great promise of BrainUGDL in utilizing individual sMRI data to make decisions about cortical functional localization for clinical populations.
- Our newly proposed Global Graph Encoding (GGE) unit innovatively introduces global encoding mechanism into current geometric deep learning framework and learns the global context information of each vertex through building and encoding the global interactions.
- Our newly proposed Local Graph Attention (LGA) unit creatively utilizes patch structure enhanced spatial information to differentiate the potential task-oriented contribution of different neighbors and learns the local context information of each vertex by aggregating the patch structure enhanced features from its spatial neighbors.
- To address the inevitable measurement noise in fMRI, an uncertainty-filtered learning mechanism is further proposed, which enables BrainUGDL to adaptively revise the fit errors of noise-containing task-fMRI labels through the estimated uncertainty, reducing the interference of noisy labels on the learning process.

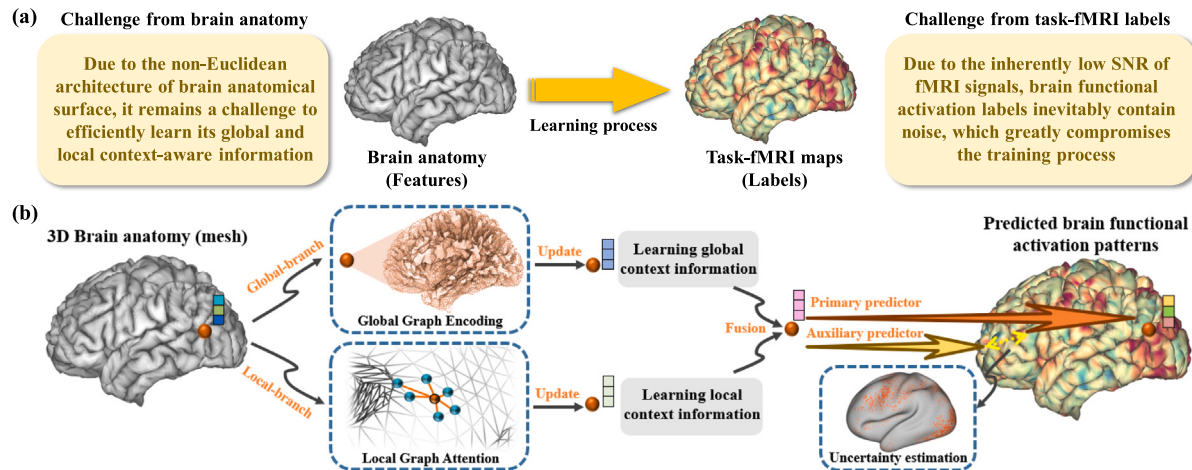


Fig. 2. (a) Challenges faced in achieving cross-modal brain anatomo-functional mapping. (b) The overall strategy of our proposed BrainUGDL: (i) By preprocessing from the raw sMRI data, the brain anatomy in medical imaging will be represented by a triangular mesh that contains vertices and connections between them, BrainUGDL directly takes the 3D brain anatomical mesh as input. (ii) The newly proposed Global Graph Encoding (GGE) unit and Local Graph Attention (LGA) unit embedded into the global branch and local branch respectively to learn global and local context-aware features of the 3D brain anatomy in a task-adaptive manner. In addition, with the newly introduced uncertainty-filtered learning mechanism, BrainUGDL can revise the influence of those task-fMRI labels with large noise, thus ensuring the effectiveness of the learning process. (iii) After iterating and updating, BrainUGDL outputs the predicted task-fMRI maps in a vertex-wise dense prediction manner.

2. Related work

2.1. Brain anatomo-functional relationship

Neuroimaging research involves exploring both anatomical and functional information over the brain, numerous studies have shown that the local and global features of brain anatomy have their own different influence on brain functions. For example, the local brain morphology or cortical thickness can be closely related to the local patterns of brain functional activation (Amiez et al., 2006; Benson et al., 2012; Amiez et al., 2013; Amiez and Petrides, 2014; Li et al., 2015; Lopez-Persson et al., 2019; Troiani et al., 2020), while the overall cortical folding pattern is related to the performance of human cognitive functions (Cash et al., 2012; Huster et al., 2011; Zhang et al., 2010; Whittle et al., 2009), or even leads to brain cognitive impairments (Willerman et al., 1991; Beaulieu et al., 2005; Simpson et al., 2012; Reardon et al., 2018). Therefore, effective extracting local and global context-aware features of brain anatomy is important to facilitate the cross-modal brain anatomo-functional mapping process.

2.2. Geometric deep learning

Geometric deep learning aims to build neural networks that can learn from non-Euclidean data, such as manifold-based brain anatomical surfaces (Bronstein et al., 2017; Gopinath et al., 2019; Cao et al., 2020; Nguyen et al., 2021; Besson et al., 2021). Although a recent study has demonstrated the applicability of geometric deep learning to predict brain function from anatomy (Ribeiro et al., 2021), they only focused on the visual cortex, whereas our task focuses on the whole brain. In current geometric deep learning framework, point-based neural network (Qi et al., 2017a,b; Ge et al., 2018; Deng et al., 2018; Zhao et al., 2021) and graph-based neural network (Monti et al., 2017; Fey et al., 2018; Verma et al., 2018; Wang et al., 2019a; Wu et al., 2020) are the two most successful technical backbones. Specifically, they are both able to handle the non-Euclidean data directly without any transformation, thus possessing the ability to extract intrinsic geometric features. Nevertheless, how to extract context-embedded features from non-Euclidean data is still a challenge for modern geometric deep learning, such as the classical PointNet (Qi et al., 2017a), which only uses a global max pooling (GMP) layer as the global feature descriptors, ignoring the global context information. Considering that both global and local features of brain anatomy will have a huge impact on brain

functions, in this work, we innovatively proposed Global Graph Encoding (GGE) unit and Local Graph Attention (LGA) unit to learn the global and local context-aware features of the 3D brain anatomy respectively in a task-adaptive manner.

2.3. Uncertainty estimation

Uncertainty estimation is widely leveraged in machine learning tasks (Kendall et al., 2015; Gal and Ghahramani, 2016; Zheng and Yang, 2021; Ju et al., 2022), since it is able to quantify the inherent noise for the given labels, thus improving the robustness of model training. For example, Kendall et al. (2015) developed a Bayesian convolutional neural network to model epistemic uncertainty and produce probabilistic pixel-wise segmentation results. Zheng and Yang (2021) leveraged the prediction variance to formulate the annotation uncertainty and involved the uncertainty into the standard cross-entropy loss to rectify the learning from noisy pseudo labels. Ju et al. (2022) used Monte-Carlo-Dropout (Gal and Ghahramani, 2016) to measure the example uncertainty and re-weighted the examples by a normalized uncertainty score to improve the robustness of the model identifying samples with label noise. Inspired by previous studies, we estimated the uncertainty of task-fMRI labels with a simple and efficient auxiliary predictor in this work and involved the uncertainty into the training process to realize revised learning from noise-containing task-fMRI labels.

3. Method

3.1. Overview

Our target is to achieve the prediction of individual-specific task-fMRI maps from the inherent brain anatomy under different cognitive task contrasts, which can be regarded as a vertex-wise dense prediction task across multiple subjects. Given a 3D brain anatomical surface/mesh with M vertices, we define the input of BrainUGDL as a $M \times 12$ matrix. That is, each specific vertex is described by a 12-dimensional vector, including its registered spatial coordinates (i.e., x , y , z) in both pial and white matter surfaces, and six other attributes (i.e., cortical thickness, sulcal depth, curvature, myelin, and neuroanatomical labels). BrainUGDL can effectively capture the mapping relationship between anatomical features and functional activation labels, and output an

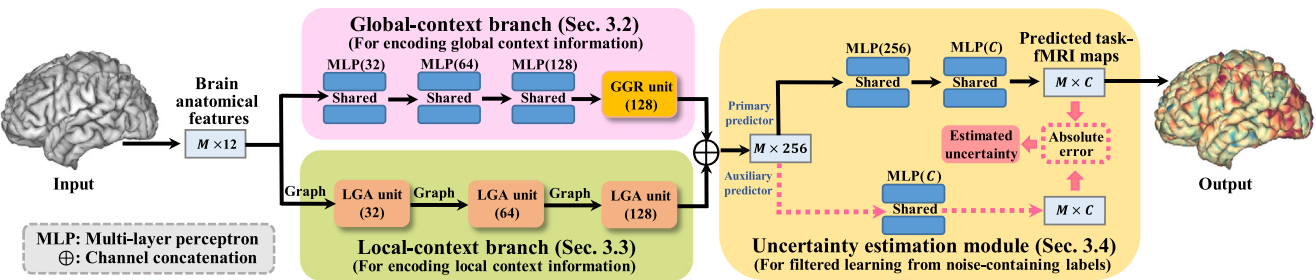


Fig. 3. Illustration of our proposed BrainUGDL, which consists of the global-context branch, the local-context branch, and the uncertainty estimation module (UEM). The number marked in parentheses for each unit represents the number of channels for its output feature map.

$M \times C$ matrix as the final predictions, where each column denotes the predicted task-fMRI maps for different cognitive task contrasts.

Our proposed BrainUGDL framework (shown in Fig. 3) contains three main parts, including the global-context branch (Section 3.2), the local-context branch (Section 3.3), and the Uncertainty Estimation Module (UEM) (Section 3.4). Suppose X_{anatomy} and Y_{function} represent the input brain anatomical features and the predicted task-fMRI maps by BrainUGDL. The raw features of brain anatomy firstly pass through two branches, the global-context branch and the local-context branch, for extracting global and local context-aware information of each vertex respectively:

$$\mathbf{F}_{\text{global}} = \mathcal{F}_{\text{global-branch}}(X_{\text{anatomy}}) \quad (2)$$

$$\mathbf{F}_{\text{local}} = \mathcal{F}_{\text{local-branch}}(X_{\text{anatomy}}) \quad (3)$$

where $\mathcal{F}_{\text{global-branch}}$ and $\mathcal{F}_{\text{local-branch}}$ are the functions of global-context branch and local-context branch respectively. The extracted global-context feature $\mathbf{F}_{\text{global}}$ and local-context feature $\mathbf{F}_{\text{local}}$ are then fused for a higher-level representation for final prediction:

$$\mathbf{F}_{\text{fusion}} = \mathbf{F}_{\text{global}} \oplus \mathbf{F}_{\text{local}} \quad (4)$$

where \oplus indicates the channel-wise concatenation. Finally, the fused feature is fed into two predictors. One named primary predictor, and the other named auxiliary predictor:

$$\hat{Y}_{\text{function}(P)} = \mathcal{F}_{\text{primary}}(\mathbf{F}_{\text{fusion}}) \quad (5)$$

$$\hat{Y}_{\text{function}(A)} = \mathcal{F}_{\text{auxiliary}}(\mathbf{F}_{\text{fusion}}) \quad (6)$$

where $\mathcal{F}_{\text{primary}}$ and $\mathcal{F}_{\text{auxiliary}}$ are the functions of primary predictor and auxiliary predictor respectively. Among them, the output from the primary predictor is the final predicted task-fMRI map, while the output from the auxiliary predictor is used for estimating the uncertainty of the noise-containing task-fMRI labels:

$$U_{\text{re}} = \mathcal{F}_{\text{uncertainty}}(\hat{Y}_{\text{function}(P)}, \hat{Y}_{\text{function}(A)}) \quad (7)$$

where $\mathcal{F}_{\text{uncertainty}}$ is the function of uncertainty estimation. By introducing the estimated uncertainty U_{re} as a regularization term into a standard regression loss, BrainUGDL can realize revised learning from the noise-containing fMRI labels to avoid interference of noisy labels on the learning process.

3.2. Global-context branch

3.2.1. Structure of global-branch

Motivated by the great potential of classical PointNet (Qi et al., 2017a) in the global representation of point sets, the global-context branch is designed with reference to the architecture of PointNet, which leverages shared multi layer perceptrons (MLPs) to learn independent feature representation of each vertex. After that, different from PointNet that uses a global max pooling (GMP) layer as the global feature descriptors, which ignores the global context information, we design

Global Graph Encoding (GGE) unit instead of the GMP layer in PointNet for achieve learning of global-context embedding features.

As shown in Fig. 3, the former part of the global-context branch consists of three MLPs, which is used for extracting increasingly higher-level features of each vertex. The number of output channels of the three MLPs is 32, 64, and 128, respectively. Each MLP is followed by batch normalization (BN) and rectified linear unit (ReLU) activation. After feature maps output from the last MLP, a GGE unit is applied to encode the global context information of the whole brain anatomy.

3.2.2. Global graph encoding (GGE) unit for learning global context features

In order to break the isolation between vertices and learn the global context embedding features for each vertex, we innovatively designed the GGE embedded into the global context branch. As shown in Fig. 4, GGE consists of two main steps: first building the affinity relationship between each vertex and all other vertices through the vertices' own features, and then encoding all the interactions through a graph convolution layer. With the help of GGE, each vertex learns the optimal global context-awareness in a task-adaptive manner, thus facilitating our vertex-wise dense prediction task.

Global graph construction. The global graph is constructed by the global relationship matrix $\tilde{A} \in \mathbb{R}^{M \times M}$, which is learnt with a parameterized dot product mechanism to adaptively build the affinity of the relationship between any two vertices. For the input feature matrix $X \in \mathbb{R}^{M \times F}$, where M is the number of the vertices, F is the feature dimensions, the process of computing \tilde{A} from the input feature matrix X is illustrated in Fig. 4, and it is formulated as:

$$\tilde{A} = \phi(X) \text{diag}(\rho(X)) \phi(X)^T \quad (8)$$

where $\phi(X) \in \mathbb{R}^{M \times F}$ is a linear embedding followed by a ReLU activation, $\rho(X) \in \mathbb{R}^{1 \times F}$ is a similar setting with the channel-wise attention proposed in Woo et al. (2018), which is consists of a global average pooling (GAP) layer and an MLP layer followed by a ReLU activation, $\phi(X)^T$ is the transpose of $\phi(X)$.

Graph encoding. After that, we perform graph encoding based on the constructed global interaction matrix \tilde{A} . The purpose of global graph encoding is to capture the relationship between any one vertex and all other vertices, which can be simplified to capture the mutual interactions between all vertex features (Chen et al., 2019). Therefore, we perform the graph encoding process with a normal graph convolution layer. Each vertex can be deemed as a node of the graph, and the global interaction matrix $\tilde{A} \in \mathbb{R}^{M \times M}$ defines the connection weights between all the nodes. Each node updated its features by aggregating information from all the other connected nodes to achieve global context-aware features. To avoid a high memory footprint on large and dense graphs, we adopt the graph convolution layer described in Welling and Kipf (2017) which can be implemented as a simple matrix multiplication without any explicit operations, this process can be formulated as:

$$\mathbf{F}_{\text{global}} = \text{Relu}(\tilde{A} X W) \quad (9)$$

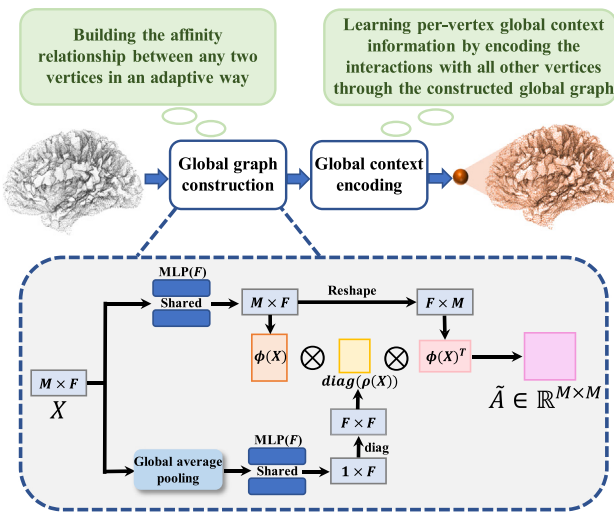


Fig. 4. The architecture of the GGE unit in the global-context branch.

where \hat{A} is the normalized form of \tilde{A} , $\hat{A} = \tilde{D}^{-\frac{1}{2}} \tilde{A} \tilde{D}^{-\frac{1}{2}}$, $\tilde{D} = \text{diag}(d_1, d_2, \dots, d_i)$, $d_i = \sum_j \tilde{A}_{ij}$, and W is a trainable weight matrix, F_{global} is the output global context-aware features. The left multiplication of the input features X by the global interaction matrix \hat{A} is performed to obtain the global context perception of all spatial vertices.

Summary of the advantages. (1) The global-context branch utilizes the classic MLP-based pipelines and the innovatively proposed GGE to extract global context-aware features of brain anatomy. (2) GGE provides an efficient and flexible way to build the global relationship in a task-adaptive manner and realizes global perception through encoding over global interactions.

3.3. Local-context branch

3.3.1. Structure of local-context branch

The local-context branch is designed with the architecture of graph-based neural network, which is particularly effective in learning local features because it updates the feature representation by aggregating the neighborhood information on a constructed graph. However, existing neighborhood information usually lacks context awareness of the overall local patch, thus, we design the LGA unit and make it as the backbone of the local-context branch. Specifically, the LGA unit uses patch structure enhanced spatial information to learn the attention coefficients, thus giving each neighbor different importance to extract more discriminating local context features.

As shown in Fig. 5, three LGA units are employed in local-context branch, the number of output channels of the three LGA units is 32, 64, and 128, respectively. Each LGA unit is followed by an exponential linear unit (ELU) activation and applied with a dropout with probability of 0.5 for its inputs.

3.3.2. Local graph attention (LGA) unit for learning local context features

Local graph construction. Since the 3D brain anatomical surface is represented by a triangular mesh composed of vertices and edges that well reflects the spatial geometry of brain anatomy (Glasser et al., 2013), therefore, unlike the global graph which is constructed based on a learning approach, our local graph $G(V, E)$ is fixed and is constructed with using the inherent edge information of the triangular mesh, where V represents the set of the M mesh vertices, E represents the set of edges. For each vertex v_i , we denote its 1-hop neighboring set (also includes v_i) in the G as \mathcal{N}_i .

Patch structure enhanced attention. In the local graph, each vertex and all its 1-hop neighboring vertices joined together can be

seen as a patch. Since graph-based neural networks update feature representations by aggregating information from neighboring nodes, therefore, enhancing the perception of neighboring vertices to the overall patch structure will be more helpful for the central vertex to obtain effective geometric information. Thus, for each center vertex v_i in G , we firstly establish the patch structure enhanced perception (PSEP) of its neighbors. Specifically, inspired by Wang et al. (2019b), we merge the feature of the center vertex into its neighbors to enhance the structure perception of the overall local patch during the information aggregation process. For each neighboring vertex $v_j \in \mathcal{N}_i$, its feature r_j with the PSEP can be formulated as:

$$r_j^{(l)} = \text{MLP}^{(l)}(f_i^{(l)} \oplus f_j^{(l)}), \forall v_j \in \mathcal{N}_i \quad (10)$$

where $f_i^{(l)}$ and $f_j^{(l)}$ denote the feature of v_i and v_j in l -th LGA unit, respectively. $\text{MLP}^{(l)} \in \mathbb{R}^{d(l+1) \times d(l)}$, $r_j^{(l)} \in \mathbb{R}^{d(l+1)}$ is the new representation of v_j with PSEP in l -th LGA unit. Then, we use r_j to compute the attention coefficient for each neighbor. Specifically, the attention coefficient $a_j^{(l)}$ is computed by applying softmax to the values computed by attention function $\varphi_\omega^{(l)}$:

$$a_j^{(l)} = \frac{\exp(\varphi_\omega^{(l)}(r_j^{(l)}))}{\sum_{k \in \mathcal{N}_i} \exp(\varphi_\omega^{(l)}(r_k^{(l)}))} \quad (11)$$

where $\varphi_\omega^{(l)}$ in our work is a single-layer feedforward neural network followed by a LeakyRelu activation (with negative input slope $\alpha = 0.2$), which can flexibly capture potential dependency between the vertices of the local spatial patch. Finally, the feature aggregation in the l -th LGA unit is formulated as:

$$f_i^{(l+1)} = \sum_{j \in \mathcal{N}_i} a_j^{(l)} r_j^{(l)} \quad (12)$$

where $f_i^{(l+1)}$ indicates the updated features of center vertex v_i , which also will be the input for the $(l+1)$ -th LGA unit.

Summary of the advantages. (1) The local-context branch uses the creatively designed LGA as the backbone to obtain local context-aware high-level feature representation through stacking LGA units. (2) LGA utilizes the information with PSEP to differentiate the potential task-oriented contribution of different neighbors and learns local context features of each vertex by selectively aggregating patch structure enhanced feature from its spatial neighbors.

3.4. Uncertainty estimation module (UEM) for achieving uncertainty-filtered learning

When recording brain functional activation patterns from an fMRI scanner, the scanner noise may interfere and change blood oxygenation level-dependent (BOLD) signals, thus leading to noise-containing labeling (Liu, 2016). The problem will be even worse at higher field strengths. To overcome the unfavorable effects of these unreliable labels on the training process, we design an Uncertainty Estimation Module (UEM), which estimates the model uncertainty with a simple and efficient way and involves the uncertainty into the optimization objective to realize the uncertainty-filtered learning mechanism. Specifically, we model the uncertainty through the approximated variance of the predicted functional activation value and involve the uncertainty as a new regularization term into the standard regression loss function to realize adaptive revised learning from the noise-containing task-fMRI labels. An intuitive illustration of the uncertainty-filtered learning mechanism can be seen in Fig. 6.

Learning with noisy labels. When dealing with continuous numeric variables, a general approach is to use a regression loss to calculate the amount of deviation of the prediction value from the underlying true value. To keep the gradient stable in the training process, we use the smooth L1 loss (Girshick, 2015) instead of the

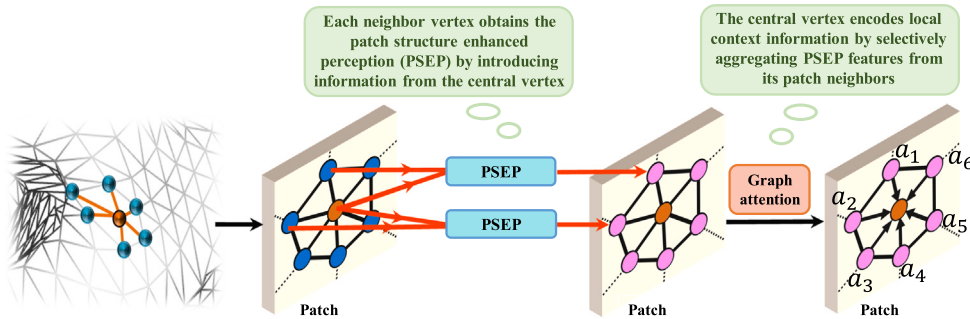


Fig. 5. The architecture of the LGA unit in the local-context branch.

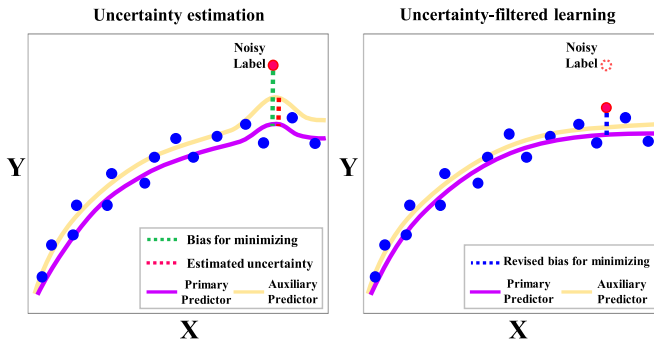


Fig. 6. An intuitive illustration of the uncertainty-filtered learning mechanism. The uncertainty is estimated by the prediction discrepancy between the primary and the auxiliary predictor, then the estimated uncertainty is formulated as a new regularization term, added into the standard regression loss to perform uncertainty-filtered learning. If the estimated uncertainty equals to zero, the uncertainty-filtered learning degrades to the objective of the conventional regression learning and the model will focus on minimizing the prediction bias only. In contrast, when the label is unreliable, the model is more likely to predict wrongly leading to a large value of estimated uncertainty, then the uncertainty-filtered learning will automatically revise the prediction bias to a smaller value based on the estimated uncertainty, thus reducing the effect of label noise on the model training.

traditional MSE loss (Allen, 1971) in our prediction task, and the smooth L1 loss can be formulated as:

$$\mathcal{L}_{(n)} = \begin{cases} 0.5(\hat{y}_n - y_n)^2, & \text{if } |\hat{y}_n - y_n| < 1 \\ |\hat{y}_n - y_n| - 0.5, & \text{otherwise} \end{cases} \quad (13)$$

where y_n is the target value, and \hat{y}_n is the prediction value. However, due to the inherent low SNR properties of fMRI signals, y_n usually inevitably contains noise. Since deep neural networks have strong memorization capacities, training the model parameter by minimizing the bias between the predictions and noise-containing labels could largely compromise the training.

Uncertainty estimation. Recently, the metric of target label noise from the perspective of uncertainty has been widely adopted by deep neural network models (Zheng and Yang, 2021; Ju et al., 2022). In our model, we design an auxiliary predictor to estimate the uncertainty. As the architecture of BrainUGDL shown in Fig. 3, in addition to the normal primary predictor, we further introduced an auxiliary predictor. The auxiliary predictor performs the same task as the primary predictor, that is, both of them will give their own predictive results for the same candidate. Because the auxiliary predictor located at a relatively shallow layer results in a different learning way from the primary predictor, and both of the two predictors apply the dropout functions (Srivastava et al., 2014), this will lead to a prediction discrepancy during training. Based on the prediction discrepancy, we can

get the approximated variance, which reflects the uncertainty of the model. To keep the same shape with the loss functions, we approximate the absolute errors of the two predictive results as the uncertainty:

$$U_n = |\hat{y}_{n(P)} - \hat{y}_{n(A)}| \quad (14)$$

where $\hat{y}_{n(P)}$ and $\hat{y}_{n(A)}$ represent the output predictions from the primary predictor and the auxiliary predictor, respectively.

Uncertainty-filtered learning mechanism. After obtaining the estimated uncertainty, we involve it as a regularization term into the smooth L1 loss function to rectify the learning from the noise-containing task-fMRI labels. If the two predictors have a large discrepancy on predictions, this reflects a large uncertainty of the model on the prediction results. By involving the uncertainty into the training target, the training process will adaptively revise the prediction bias to a smaller value to reduce the interference of noisy labels on the learning process. The uncertainty-filtered smooth L1 loss can be formulated as:

$$\mathcal{L}_{U(n)} = \begin{cases} 0.5(|\hat{y}_n - y_n| - U_n)^2, & \text{if } ||\hat{y}_n - y_n| - U_n| < 1 \\ ||\hat{y}_n - y_n| - U_n| - 0.5, & \text{otherwise} \end{cases} \quad (15)$$

To prevent a large uncertainty from always existing, we extra add the uncertainty itself U_n into loss function as a trade-off. Thus, the uncertainty-filtered smooth L1 loss finally used in our model can be formulated as:

$$\mathcal{L}_{U(n)} = \begin{cases} 0.5(|\hat{y}_n - y_n| - U_n)^2 + U_n, & \text{if } ||\hat{y}_n - y_n| - U_n| < 1 \\ ||\hat{y}_n - y_n| - U_n| - 0.5 + U_n, & \text{otherwise} \end{cases} \quad (16)$$

It is worth noting that both the primary predictor and auxiliary predictor are involved with the designed $\mathcal{L}_{U(n)}$ loss, so $\hat{y}_n \in \{\hat{y}_{n(P)}, \hat{y}_{n(A)}\}$. But only the outputs from the primary predictor are used as our prediction results, to keep the prediction responsibility of the primary predictor, the auxiliary predictor is only valid during training and its training weight is smaller than the primary predictor. The PyTorch-style pseudocode of the uncertainty-filtered regression mechanism can be seen in supplemental Algorithm S1.

Summary of advantages. (1) UEM designs a low-cost and efficient auxiliary predictor to estimate the vertex-wise uncertainty map by computing the prediction discrepancy with the primary predictor. (2) The estimated uncertainty has the same shape with the standard regression loss function, by formulating the estimated uncertainty as a new regularization item into the standard smooth L1 loss, BrainUGDL could perform vertex-wise revised learning from the noise-containing task-fMRI labels.

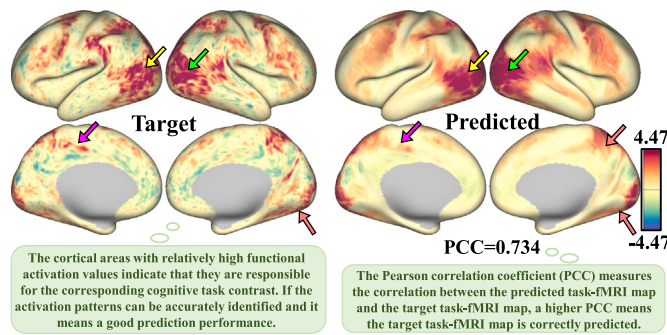


Fig. 7. Description of the predictive outcomes and the *PCC* evaluation metric. For easy observation of the cortical areas, inflated views of the cortical surfaces are shown.

4. Experimental results

4.1. Data and implementation details

We benchmark our performance using preprocessed sMRI and task-fMRI data from the publicly released HCP.¹ The subjects were 22 to 35 years old and scanned using Washington University's 3T Siemens Connectome Scanner (Van Essen et al., 2012). Following the minimal preprocessing pipelines of HCP (Glasser et al., 2013), each individual's native space was registered to the MNI space by applying the volume-based affine transformation, then was registered to *fs_LR_32k* surface template with 32,492 vertices of each hemisphere using the rigid surface-based transformation provided by FreeSurfer and MS-Mall (Coalson et al., 2018). Due to the medial wall does not contain cortical gray matter, therefore, 29,696 out of 32,492 vertices for the left hemisphere and 29,716 out of 32,492 vertices for the right hemisphere were practically selected. In our experiment, those classic brain anatomical features provided by the FreeSurfer (Fischl, 2012) were used as the input, specifically, these anatomical features include each vertex's spatial location on both inner and outer cortical surfaces (i.e., *x*, *y* and *z* coordinates of both white matter and pial surfaces), and six other attributes included cortical thickness, sulcal depth, curvature, myelin (determined by the ratio of T1w/T2w images) and the neuroanatomical labels in both Desikan atlas (Desikan et al., 2006) and Destrieux atlas (Destrieux et al., 2010). It is worth noting that all of these features are derived only from the sMRI without containing any functional information.

Of the 86 contrasts across 7 task domains included in HCP, 47 unique contrasts were included in our experiments (shown in Table 1), as the remaining 39 were just sign-reversed contrasts. Considering the completeness of the required 47 unique contrasts, we finally screened 958 of the 1206 subjects released from HCP for our experimental data. Among the 958 subjects, 919 with only one scan measurement were used for training, and the other 39 with two scan measurements were used for validation/testing, as using the average of the two measurements is considered to be a more reliable test label, which could better validate the training effectiveness of our model under noise-containing labels. To improve generalization, we performed data augmentation on the training set by rotating each brain anatomical mesh around *x*-, *y*- or *z*-axis with randomly sampling angles between $[\pi/4, -\pi/4]$.

All our experimental implementations used PyTorch on a GPU of Nvidia Tesla V100 with a memory of 32 GB. The training was carried out for 200 epochs with a batch size of 1 and a learning rate at 0.001 for 100 epochs that was then adjusted to 0.0002, using Adam optimizer. The weight coefficient of auxiliary predictor in the loss function was set to 0.5. The best models were saved based on validation

Table 1
Illustration of the 47 contrasts involved in our experiment.

Task domain	Contrast
WM	1) 2BK_BODY
	2) 2BK_FACE
	3) 2BK_PLACE
	4) 2BK_TOOL
	5) 0BK_BODY
	6) 0BK_FACE
	7) 0BK_PLACE
	8) 0BK_TOOL
	9) 2BK
	10) 0BK
MOTOR (MOT)	11) 2BK-0BK
	12) BODY
	13) 0BK
	14) PLACE
	15) TOOL
LANGUAGE (LANG)	16) BODY-AVG
	17) FACE-AVG
	18) PLACE-AVG
	19) TOOL-AVG
	1) UE
RELATIONAL (RELA)	2) LF
	3) LH
	4) RF
	5) RH
	6) T
SOCIAL (SOC)	7) AVG
	8) CUE-AVG
	9) LF-AVG
EMOTION (EMO)	10) LH-AVG
	11) RF-AVG
	12) RH-AVG
GAMBLING (GAM)	13) T-AVG
	1) MATH
	2) STORY
RELATIONAL (RELA)	3) MATH-STORY
	1) MATCH
	2) REL
SOCIAL (SOC)	3) MATCH-REL
	1) RANDOM
	2) TOM
EMOTION (EMO)	3) RANDOM-TOM
	1) FACES
	2) SHAPES
GAMBLING (GAM)	3) FACES-SHAPES
	1) PUNISH
	2) REWARD
GAMBLING (GAM)	3) PUNISH-Reward

data while keeping the evaluation data untouched. Similar with Tavor et al. (2016), Pearson correlation coefficient (*PCC*) was used as the evaluation metric for our prediction performance, and the *PCC* was calculated as follows:

$$PCC_{(\hat{Y}_{(i)}, Y_{(i)})} = \frac{\text{cov}(\hat{Y}_{(i)}, Y_{(i)})}{\sigma_{\hat{Y}_{(i)}} \sigma_{Y_{(i)}}} \quad (17)$$

where $\hat{Y}_{(i)}$ and $Y_{(i)}$ represent the individual predicted task-fMRI maps and the target task-fMRI maps, respectively. More details about the *PCC* evaluation metric are described in Fig. 7.

4.2. Training process and sensitivity on sample size

In Fig. 8, we randomly select the LANGUAGE (MATH-STORY) contrast as a showcase example to illustrate the evolution of BrainUGDL over iterations and its sensitivity to sample size. As we can see in Fig. 8(a), the predicted task-fMRI maps gradually tends to be consistent with the target in the training process, which shows the effectiveness of our framework. As the training progresses, the accuracy on both training and testing datasets converges smoothly (Fig. 8(b)), which shows that the training strategy is appropriate. The sensitivity of BrainUGDL on sample size was shown in (Fig. 8(c)), the number of training set was ranged from 5 to 919 with a smaller step before the plateau and a larger step after. It can be found that the performance reached a plateau of 0.68 with around 100 subjects. After that, performance only showed slight improvement by using larger data sample size.

4.3. Comparison with other potential competitors

4.3.1. Quantitative evaluation demonstrates our advantages

To verify the advantages of our proposed BrainUGDL, comparison experiments are conducted between BrainUGDL and five other potential competitors. For a fair comparison, all the compared methods share the same input anatomical features with our BrainUGDL. These potential competitors can be grouped into the following three categories:

(1) **Feature-based methods:** such as ordinary least squares regression (OLSR), which is often used in neuroscience in a piece-wise manner (Kannurpatti and Biswal, 2012; Tavor et al., 2016). This method absolutely rely on these hand-extracted features and model each vertex independently.

(2) **CNN-based learning methods:** such as Spherical U-Net (Zhao et al., 2019), which extends the pooling architecture of U-Net to the icosahedron-like spherical convolution fields. Since the underlying structure of *fs_LR_32K* template is derived from an icosahedron, thus Spherical U-Net can model the registered brain anatomical surface.

¹ <https://www.humanconnectome.org/study/hcp-young-adult>

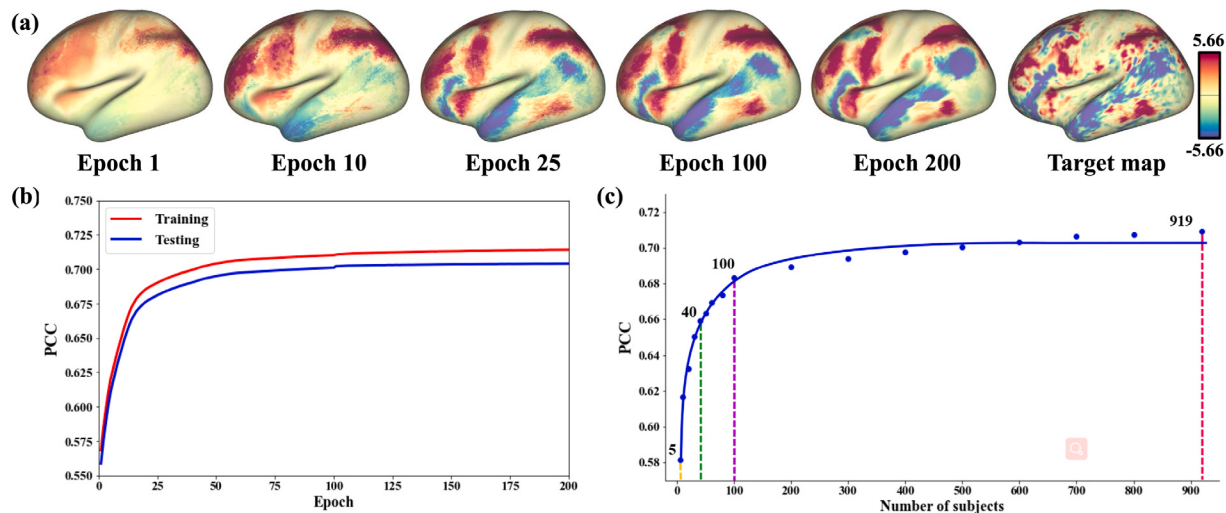


Fig. 8. (a) The predicted task-fMRI maps for the LANGUAGE (MATH-STORY) contrast over multiple epochs are shown. For easy observation of the cortical areas, inflated views of the cortical surfaces are shown. (b–c) The convergence analysis and sample-size effect analysis of BrainUGDL for the LANGUAGE (MATH-STORY) contrast.

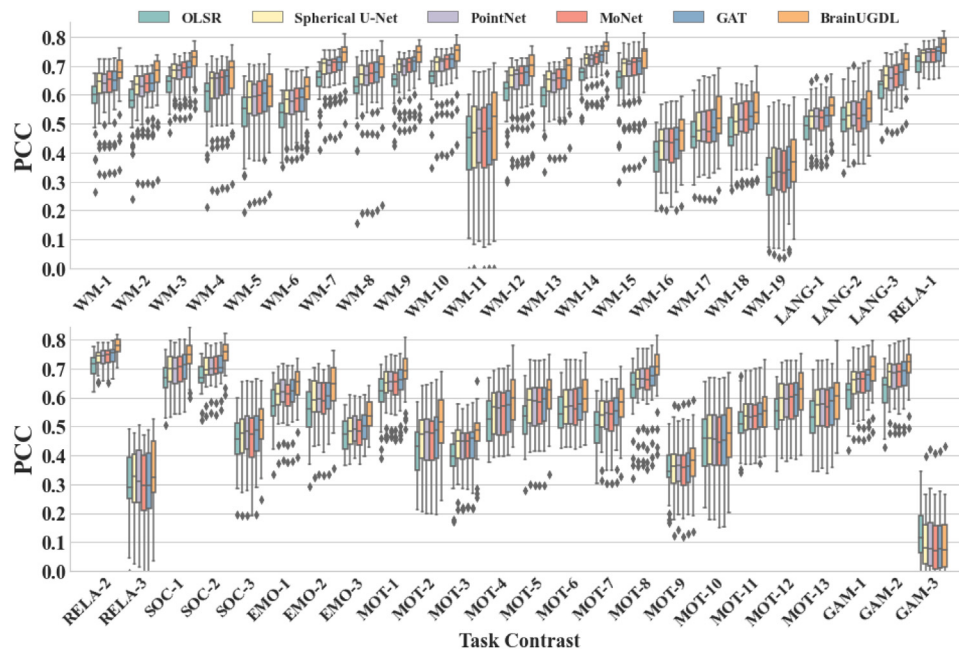


Fig. 9. Prediction performance measured by PCC between BrainUGDL and other potential competitors on all the 47 unique contrasts. BrainUGDL outperforms the competitors in all cases except for the GAMBLING (PUNISH-REWARD) contrast, since the activations of the GAMBLING (PUNISH-REWARD) contrast are restricted to sub-cortical gray matter. The corresponding task name abbreviations and contrast labels can be found in Table 1.

However, due to the different neighborhood structure of each vertex in fs_LR 32K template (e.g., the initial 12 vertices have five direct neighbors and the remaining have 6 direct neighbors, and the medial wall further breaks its regular neighborhood structure), therefore, Spherical U-Net relies on manual convolutional kernel definitions to fit the different neighborhood structures of each vertex.

(3) **Geometric deep learning methods:** such as PointNet (Qi et al., 2017a), MoNet (Monti et al., 2017) and Graph AttenTion network (GAT) (Veličković et al., 2017; Wang et al., 2019a), which are the most representative techniques in geometric deep learning today, and achieve state-of-the-art performance in 3D computer vision. Specifically, PointNet encodes each vertex individually with shared MLPs, MoNet parameterizes local representations using pseudo-coordinates around each vertex, GAT utilizes learnable kernel shapes to dynamically adapt to the local structure of each vertex. These methods are similar to our BrainUGDL that are able to deal with the registered brain

anatomical surface directly without any manual convolutional kernel definitions.

The prediction performance of BrainUGDL and the five potential competitors for all the 47 unique contrasts across the 7 cognitive task domains are shown in Fig. 9. Due to the activations of the GAMBLING (PUNISH-REWARD) contrast are restricted to sub-cortical gray matter (Tavor et al., 2016), whereas our experiments only make prediction for the cerebral cortex, thus, the prediction results for this contrast have no comparability, and we exclude the statistical results for the GAMBLING (PUNISH-REWARD) contrast in the subsequent figures and tables.

In the remaining 46 contrasts, it is easy to observe that the learning-based approaches are generally superior to the feature-based approach, which indicates that by capturing context information, the learning-based approach can better learn task-oriented feature representations of each vertex, thus improving the performance of the

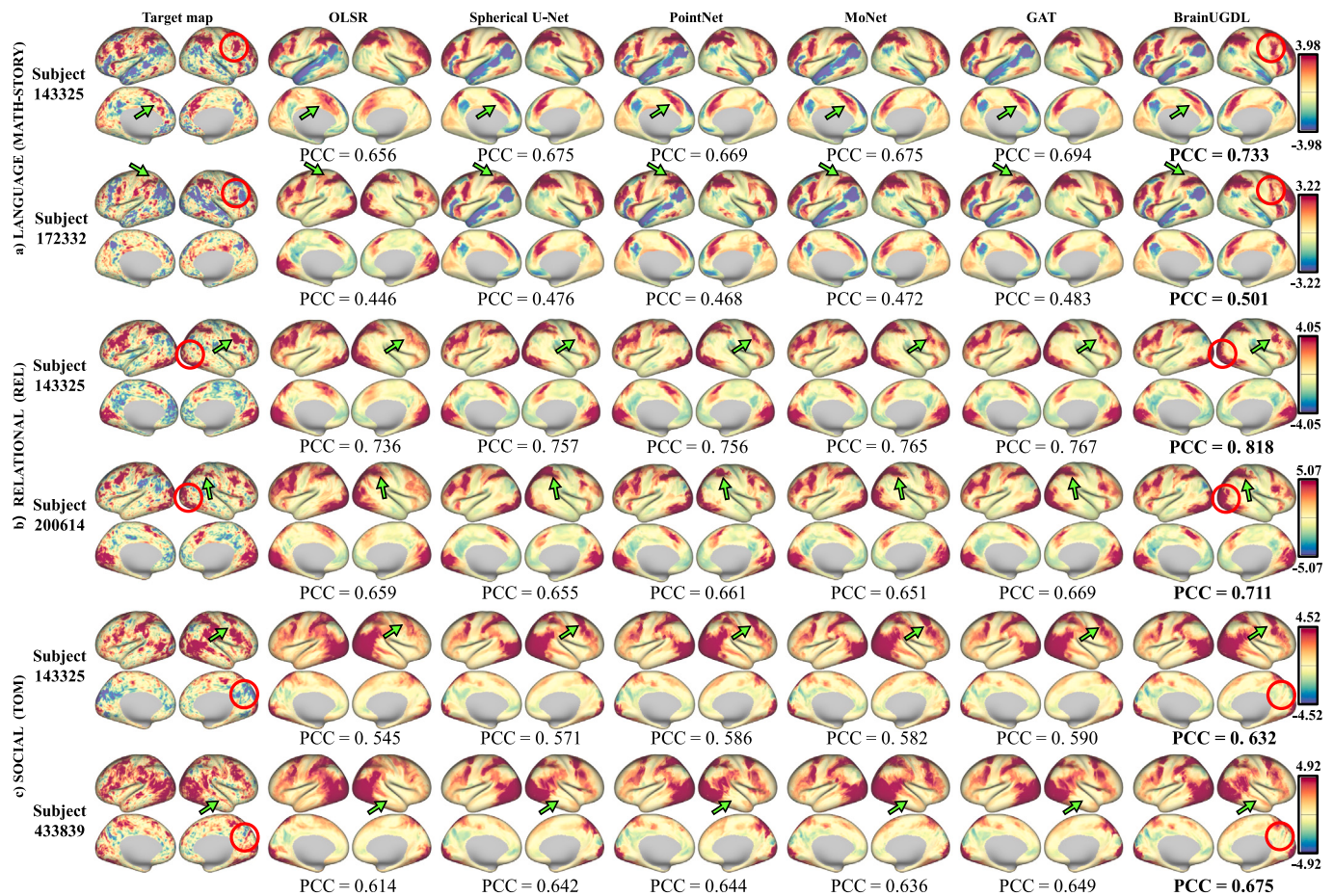


Fig. 10. The visual comparisons between BrainUGDL and other five potential competitors on the LANGUAGE (MATH-STORY), RELATIONAL (REL), SOCIAL (TOM) contrasts. For each contrast, two subjects are in consideration, one is to randomly select from the test subjects as a fixed reference, e.g., “143325”, and the other is to select the test subjects with the lowest correlation with the reference subject, so as to allow individual differences between the two subjects. The green arrows highlight where our method predicts more accurately than the potential competitors for the same example case, and the red circles highlight those cortical activation patterns that differ individually but can still be accurately predicted. For easy observation of the cortical areas, inflated views of the cortical surfaces are shown.

vertex-wise prediction task. Among the learning-based methods, Spherical U-Net, PointNet, MoNet, and GAT have similar performance, but with slight difference on different contrasts, which illustrates that these methods have comparable ability to capture context information, and their different kernel architectures result in slightly different performance in the face of different contrasts. Finally, compared with Spherical U-Net, PointNet, MoNet and GAT, our BrainUGDL achieves the best prediction performance and significantly outperforms all other potential competitors on 19 of them (Supplemental Table S1), suggesting that our designed simultaneous global and local context feature extraction is appropriate and necessary for the in-depth understanding of brain anatomo-functional relationship, and that the designed uncertainty-filtered learning mechanism further powers the brain cross-modal anatomo-functional prediction process. The same comparative results can also be observed on another metric (Supplemental Fig. S1), the whole-brain R^2 -score (Dohmatob et al., 2021), where BrainUGDL outperforms other potential competitors and still achieves significant improvements on 9 of these contrasts (Supplemental Table S2), indicating that the improved performance of our approach is not limited to the choice of PCC as our evaluation metric.

4.3.2. Qualitative evaluation shows our visual superiority

Fig. 10 shows the visual comparisons between BrainUGDL and other five potential competitors. The showcase example contrasts in consideration include LANGUAGE (MATH-STORY), RELATIONAL (REL) and SOCIAL (TOM) contrasts, which have the highest level of significant improvement among all the contrasts (Table S1). Each showcase contrast

includes two subjects, one is to randomly select from the test subjects as a fixed reference, e.g., “143325”, and the other is to select the test subjects with the lowest correlation with the reference subject, so as to allow individual differences between the two subjects.

(1) Predictable activation patterns: As shown in Fig. 10, due to the lack of ability to extract high-level context information, OLSR performs rough predictions, especially in RELATIONAL (REL), whose activation pattern is fragmented-like in the frontal lobe. With the ability to extract anatomical context, Spherical U-Net, PointNet, MoNet, and GAT achieve more accurate predictions than OLSR, but they lose some important details (highlighted by green arrows in Fig. 10). Due to the positive effect of simultaneous global and local context information extraction and effective uncertainty-filtered learning mechanism, our BrainUGDL is more sensitive to these details and obtains the best prediction performance.

(2) Captureable individual differences: As shown in the highlighted red circles of Fig. 10, although there are different activation patterns between different subjects under the same contrast, BrainUGDL can also accurately capture the individual differences, which indicates that BrainUGDL is able to capture such subject-specific characteristics during the prediction process.

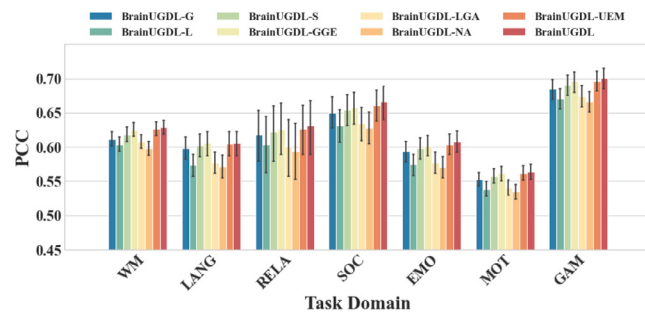


Fig. 11. Results summary of ablation analysis on each key component of BrainUGDL. The results show that each key component designed in our BrainUGDL has a positive contribution to the cross-modal brain anatomo-functional mapping tasks.

4.4. Ablation analysis

An ablation analysis is performed to explore and validate our designed key components in BrainUGDL as Section 3 mentioned. Specifically, we evaluate the influence of the architecture of global-local dual branches, the newly designed GGE unit, LGA unit, and UEM.

4.4.1. Effectiveness of the dual-branch structure

Considering that both global and local structures of brain anatomy have an impact on brain functions from their respective perspectives, our BrainUGDL is designed with two parallel branches that integrates the advantages of the two different geometric deep learning technologies into a unified framework to encode the global context information and local context information, respectively.

To verify the effectiveness of the dual-branch architecture in our model, we design a set of comparative experiments to compare the performance with removing the global-context branch or the local-context branch to generate two different variants of BrainUGDL, which are denoted as BrainUGDL-G and BrainUGDL-L, respectively. In addition, we also build another single-branch variant of BrainUGDL (denoted as BrainUGDL-S) by concatenating the local-context branch and global-context branch in sequence. The comparative results between these simplified models are shown in Fig. 11. It can be seen that BrainUGDL-G and BrainUGDL-L lead to worse results than both BrainUGDL-S and BrainUGDL. This justifies the complementarity between the geometric information provided by the global-context branch and the local-context branch in delineating brain anatomy. On the other hand, when compared with BrainUGDL-S, the original two-branched BrainUGDL has better predictive accuracy, which suggests that our design of two parallel branches to extract purely global and local context features on their own views respectively is more conducive to our brain anatomo-functional mapping task. In addition, as shown in Fig. 12, the t-SNE visualization of the output features of the two branches also indicates a similar conclusion that the features extracted by the two branches are complementary and can provide more power for the cross-modal brain anatomo-functional predictions.

4.4.2. Effectiveness of GGE unit and LGA unit designs

As the two core designs of BrainUGDL, GGE unit and LGA unit are embedded into two different branches to encode the global context feature and local context feature, respectively. For ablation analysis, we remove them respectively to validate the effects of the GGE unit and LGA unit in our task. We denote BrainUGDL-GGE to represent the model removing GGE unit from the global-context branch by replacing it with a Global Maximum Pooling (GMP) layer used in PointNet (Qi et al., 2017a). Similarly, we denote BrainUGDL-LGA to represent the model removing LGA unit from the local-context branch by replacing it with a standard Graph AttenTion (GAT) layer (Veličković et al., 2017). We also denote BrainUGDL-NA to represent the model with

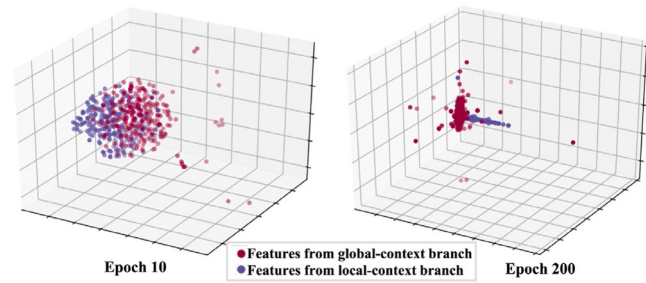


Fig. 12. The t-SNE visualization of the output features from global-context branch and local-context branch. The visualization indicates that the features extracted by the two branches are complementary and can provide more power for the cross-modal brain anatomo-functional predictions.

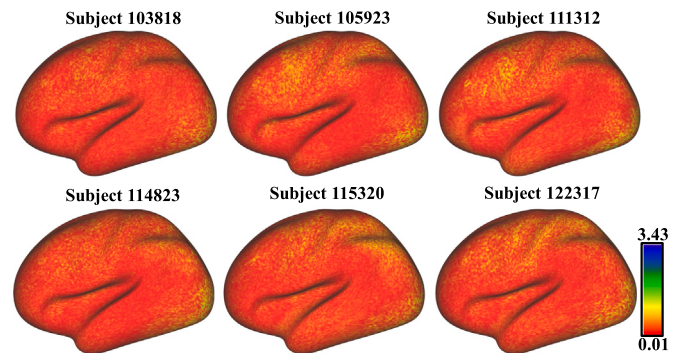


Fig. 13. Visualization of the uncertainty estimation distribution of six different subjects for the MOTOR(CUE-AVE) contrast. For easy observation of the cortical areas, inflated views of the cortical surfaces are shown. It can be seen that the task-fMRI labels with high uncertainty are with great differences in distribution across individuals, and the uncertainty-filtered learning of UEM could adaptively revise the bias of these high-uncertainty labels to make the model less disturbed by these noisy labels during the training process.

both GGE and LGA replaced. We compare these three variants with the original BrainUGDL and present the quantitative results listed in Fig. 11. The results show that: removing arbitrary design causes a decline in performance, and the decline is more pronounced if both are removed, suggesting the importance of both GGE and LGA units.

4.4.3. Effectiveness of the UEM

As described in Section 3.4, we design UEM to estimate the model uncertainty by predicting the variance and involve the estimated uncertainty in the optimization objective to realize revised learning from the noise-containing task-fMRI labels. We randomly selected the MOTOR(CUE-AVE) contrast as a showcase example to visualize the uncertainty estimation distribution of six different training subjects in Fig. 13. It can be seen that the task-fMRI labels with high uncertainty are with great differences in distribution across individuals, and the uncertainty-filtered learning of UEM could adaptively revise the bias of these high-uncertainty labels to make the model less disturbed by these noisy labels during the training process. To evaluate the effectiveness of our UEM design, we quantify the performance of BrainUGDL by removing the UEM (BrainUGDL-UEM). As shown in Fig. 11, we can observe that the UEM designed in BrainUGDL has a positive effect on performance, which indicates that paying attention to the noise of fMRI is essential to improve prediction performance.

4.5. Individual identification

There are individual differences in human brain functional activation patterns, that is to say, even under the same cognitive task contrast,

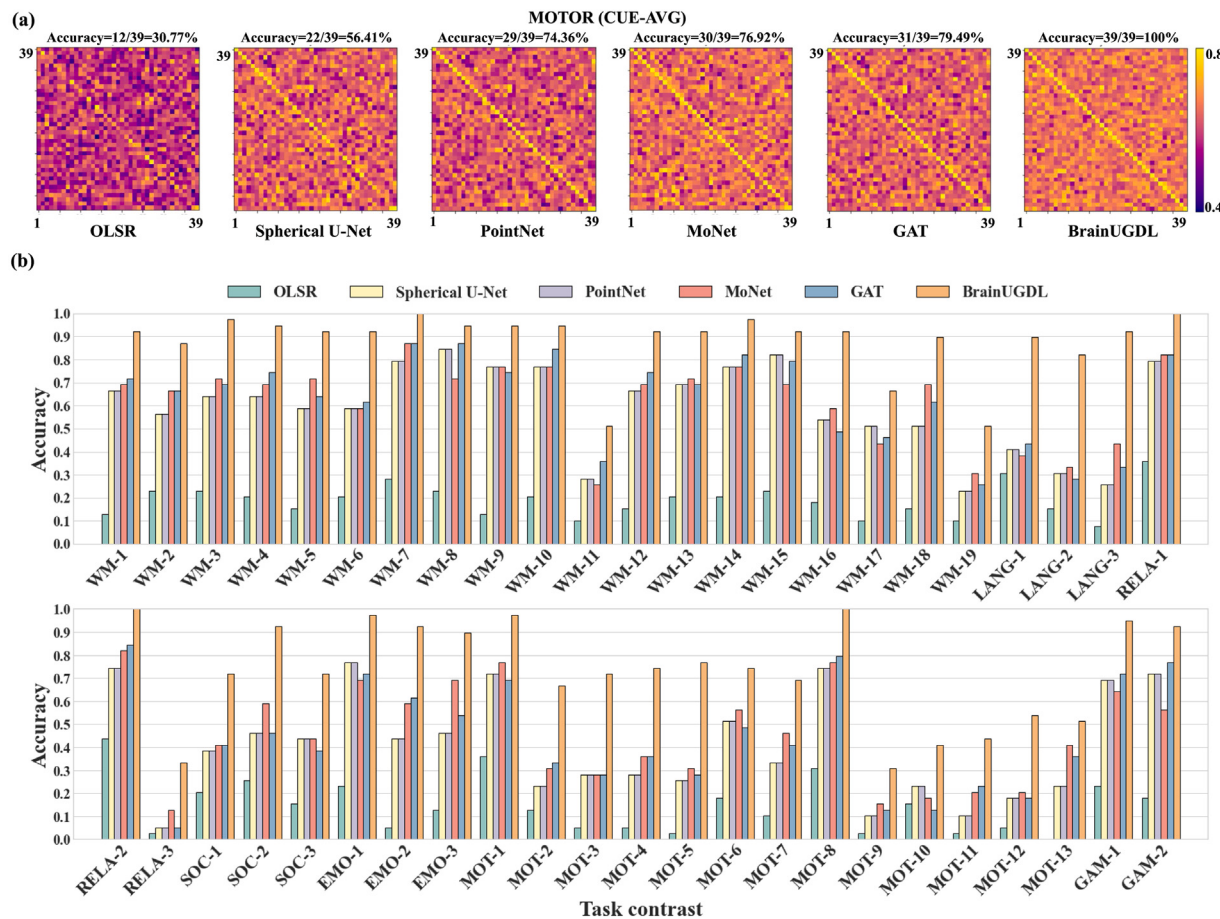


Fig. 14. (a) BrainUGDL has the best performance of individual identification in the anatomo-functional prediction process. Correlation matrices for the MOTOR(CUE-AVE) contrast between the predicted activation maps and the actual measured activation maps across the 39 test subjects are shown. The more obvious diagonal indicates that the predicted activation map is only the most similar to itself, that is, the higher accuracy of individual identification. (b) The comparison of individual identification accuracy between BrainUGDL and other potential competitors across the 39 test subjects. BrainUGDL outperforms other competitors by a large margin. The corresponding task name abbreviations and contrast labels can be found in Table 1.

the task-fMRI maps of each subject present more or less subtle differences (Barch et al., 2013). As a result, the human functional profiles sometimes are also called “fingerprints” that can reflect the individual’s biological information (Finn et al., 2015; Guedj and Vuilleumier, 2020). Therefore, it has important significance to make the prediction have better individual identification performance (Tavor et al., 2016).

We utilize the predicted task-fMRI maps to verify the ability for individual identification, and BrainUGDL is significantly superior to other competitors. We randomly select the MOTOR (CUE-AVE) contrast as a showcase example to show the correlation matrices across the 39 test subjects in Fig. 14(a). The 39 by 39 correlation matrix reflects the correlation between each subject’s predicted task-fMRI maps (columns) and all other subjects’ (contains himself) actual measured task-fMRI maps (rows). If the i -th element of the i -th row has the highest value, it means that the i -th subject can be identified accurately among all test subjects by the predicted task-fMRI maps. Similar to Tavor et al. (2016), the matrices are normalized for clearly visualizing the higher variability. It can be easily seen that the diagonal line of BrainUGDL is more obvious compared to other competitors, which means that BrainUGDL has better performance in individual identification. Fig. 14(b) shows the accuracy of individual identification for the 46 contrasts. Compared with other competitors, BrainUGDL has better individual identification accuracy, indicating that the powerful learning ability of BrainUGDL greatly facilitates the capture of individual differences, i.e., the different performances of different subjects under the same contrast.

5. Discussion

5.1. Test-retest reliability

The intraclass correlation coefficient (ICC) is a prominent statistic to measure test-retest reliability of task-fMRI data (Zuo et al., 2010). The test-retest reliability analysis was performed on the actual measured task-fMRI maps and BrainUGDL predictions by calculating the ICC using the ICC (3,1) mixed-effects model defined in Shrout and Fleiss (1979). As shown in Fig. 15(a), the 39 test subjects involved in our experiment were used for evaluated the test-retest reliability since they had repeated measures sMRI and task-fMRI data. The repeated measures data were collected in exactly the same way as the initial, but four months later. The results are shown in Fig. 15(b), the BrainUGDL predicted task-fMRI maps have excellently higher ICCs than that of the actual measured task-fMRI maps, which shows the great potential of BrainUGDL to improve the low reliability of fMRI in clinical applications.

5.2. sMRI vs. resting-fMRI

Considering the inherent close relationship between brain anatomy and its functional activity, a major motivation of our work is the effort to achieve the prediction of task-fMRI maps solely from individual brain sMRI data. Beside this, another common approach is to use resting-fMRI data to predict task-fMRI maps (Tavor et al., 2016; Ngo et al., 2022), since resting-fMRI is regarded as to reveal the intrinsic

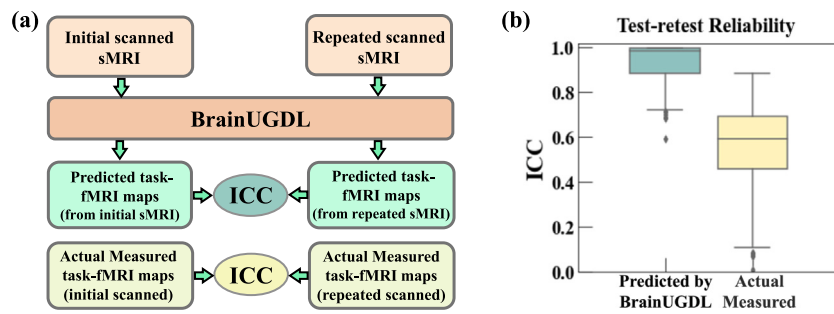


Fig. 15. (a) The test–retest reliability analysis was performed by evaluating ICC on the BrainUGDL predicted maps and the actual measured maps. (b) The predicted task-fMRI maps got by BrainUGDL have higher ICC scores than that of the actual measured task-fMRI maps, which suggests that BrainUGDL has great potential in improving the low reliability of fMRI in clinical applications.

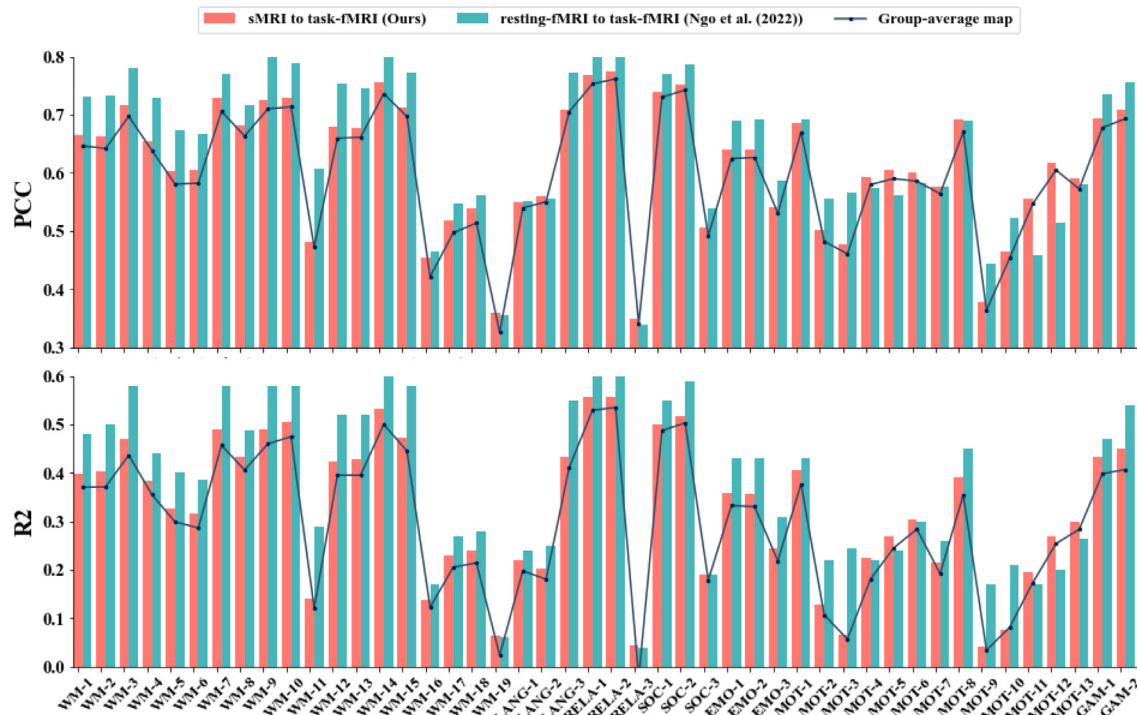


Fig. 16. The mapping performances of sMRI to task-fMRI (ours) and resting-fMRI to task-fMRI (Ngo et al., 2022) on PCC and whole-brain R^2 -score metrics. The corresponding task name abbreviations and contrast labels can be found in Table 1.

functional organization of the human brain (Cole et al., 2016). Thus, we compared our work with Ngo et al. (2022). Specifically, we have the same prediction targets, that is the task-fMRI maps, but the difference is that Ngo et al. (2022) is based on the resting-fMRI, which is an intra-modal mapping, and we are wholly based on sMRI, which is a cross-modal mapping.

Fig. 16 shows the prediction performances of these two approaches on PCC and whole-brain R^2 -score metrics. It is easy to observe that their prediction results have a high trend of consistency in the two metrics, which indicates that brain anatomical features and resting brain functional features share a mutual basis in characterizing human higher cognitive activities. A potential possibility is that the brain anatomical features determine its resting functional activity patterns, which in turn further determine human higher cognitive activities (Zamboni et al., 2013; Van Tol et al., 2014). Besides, we also involved the group-average map as a naive reference, since it reflects the most salient features for a given contrast activation pattern. It can be seen that the salient features for most contrasts can be captured by both of the two approaches. Although the prediction method based on resting-fMRI has a slight superiority, as resting-fMRI and task-fMRI belong to the

same modality and have closely related, it is not surprising that the prediction performances based on resting-fMRI are generally higher than that of sMRI. Even so, in some contrasts of the MOTOR task (e.g., MOTOR (RF, RH, T, RF-AVG, RH-AVG, T-AVG)), the prediction performance based on sMRI outperforms that based on resting-fMRI, which indicates that our approach has its unique and irreplaceable advantages. In addition, compare to fMRI, sMRI is easier to collect and does not require subjects to have cognitive abilities, making it easier to generalize in clinical applications.

5.3. Limitation and future work

Although BrainUGDL obtained promising outcomes for cross-modal brain anatomo-functional predictions, there are still some limitations to be considered in this study. For example, here we only focused on external anatomical features of the brain, and did not pay more attention to the internal anatomical indicators, such as the white matter fibers, which are thought to play a role in communication (Zhang and Sejnowski, 2000). The main reason for this is that the spatial resolution of the available neuroimaging data is insufficient to fully understand

the orientation of white matter fiber bundles (Liu et al., 2020). In our future work, we will work to continuously improve and optimize the performance of the brain anatomo-functional mapping model and attempt to extend this analysis to brain disease to explore the potential anatomo-functional associations, since both brain anatomical structures and cognitive functions of Alzheimer's disease are impaired with disease progression (Kulason et al., 2019).

6. Conclusion

In this work, we have proposed a novel unified geometric deep learning framework (BrainUGDL) to perform the cross-modal brain anatomo-functional mapping. It can directly process the 3D brain anatomy as input, and output the predicted task-fMRI maps comparable to the actual measured. On one hand, considering that both global and local structures of brain anatomy have an impact on brain functions from their respective perspectives, BrainUGDL is designed with an effective global-context and local-context extraction mechanism for the 3D brain anatomy and demonstrates its superiority through extensive ablation analysis. On the other hand, considering the inevitable measurement noise in task-fMRI labels, an uncertainty-filtered learning mechanism is further proposed that enables BrainUGDL to achieve adaptive revised learning from the noise-containing task-fMRI labels. Experiments across seven open task-fMRI datasets from HCP demonstrate that our BrainUGDL outperforms other potential competitors by a large margin. BrainUGDL's excellent performance makes it promising to use sMRI data to make clinical decisions about individual cortical functional localizations.

Declaration of competing interest

The authors declare that they have no known competing financial interests or personal relationships that could have appeared to influence the work reported in this paper.

Data availability

The authors do not have permission to share data.

Acknowledgment

This work was supported by the General Program of National Natural Science Foundation of China (Grant No. 61876021), the General Program of Beijing Natural Science Foundation (Grant No. 4212037) and the program of China Scholarship Council (No. 201906040187). We thank the HCP projects for sharing their valuable sMRI and task-fMRI datasets.

Appendix A. Supplementary data

Supplementary material related to this article can be found online at <https://doi.org/10.1016/j.media.2022.102681>.

References

- Allen, D.M., 1971. Mean square error of prediction as a criterion for selecting variables. *Technometrics* 13 (3), 469–475.
- Amiez, C., Kostopoulos, P., Champod, A.-S., Petrides, M., 2006. Local morphology predicts functional organization of the dorsal premotor region in the human brain. *J. Neurosci.* 26 (10), 2724–2731.
- Amiez, C., Neveu, R., Warrot, D., Petrides, M., Knoblauch, K., Procyk, E., 2013. The location of feedback-related activity in the midcingulate cortex is predicted by local morphology. *J. Neurosci.* 33 (5), 2217–2228.
- Amiez, C., Petrides, M., 2014. Neuroimaging evidence of the anatomo-functional organization of the human cingulate motor areas. *Cerebral Cortex* 24 (3), 563–578.
- Amiez, C., Petrides, M., 2018. Functional rostro-caudal gradient in the human posterior lateral frontal cortex. *Brain Struct. Funct.* 223 (3), 1487–1499.
- Barch, D.M., Burgess, G.C., Harms, M.P., Petersen, S.E., Schlaggar, B.L., Corbetta, M., Glasser, M.F., Curtiss, S., Dixit, S., Feldt, C., et al., 2013. Function in the human connectome: task-fMRI and individual differences in behavior. *Neuroimage* 80, 169–189.
- Beaulieu, C., Plewes, C., Paulson, L.A., Roy, D., Snook, L., Concha, L., Phillips, L., 2005. Imaging brain connectivity in children with diverse reading ability. *Neuroimage* 25 (4), 1266–1271.
- Benson, N.C., Butt, O.H., Datta, R., Radovcic, P.D., Brainard, D.H., Aguirre, G.K., 2012. The retinotopic organization of striate cortex is well predicted by surface topology. *Curr. Biol.* 22 (21), 2081–2085.
- Besson, P., Parrish, T., Katsaggelos, A.K., Bandt, S.K., 2021. Geometric deep learning on brain shape predicts sex and age. *Comput. Med. Imaging Graph.* 101939.
- Biswal, B., Deyoe, E.A., Hyde, J.S., 1996. Reduction of physiological fluctuations in fMRI using digital filters. *Magn. Reson. Med.* 35 (1), 107–113.
- Bronstein, M.M., Bruna, J., LeCun, Y., Szlam, A., Vandergheynst, P., 2017. Geometric deep learning: going beyond euclidean data. *IEEE Signal Process. Mag.* 34 (4), 18–42.
- Buddy, S., Steinmann III, P., Kuhl, E., 2015. Physical biology of human brain development. *Front. Cellular Neurosci.* 9, 257.
- Calhoun, V., 2018. Data-driven approaches for identifying links between brain structure and function in health and disease. *Dialogues Clin. Neurosci.* 20 (2), 87.
- Cao, W., Yan, Z., He, Z., He, Z., 2020. A comprehensive survey on geometric deep learning. *IEEE Access* 8, 35929–35949.
- Cash, D.M., Melbourne, A., Modat, M., Cardoso, M.J., Clarkson, M.J., Fox, N.C., Ourselin, S., 2012. Cortical folding analysis on patients with Alzheimer's disease and mild cognitive impairment. In: International Conference on Medical Image Computing and Computer-Assisted Intervention. Springer, pp. 289–296.
- Chen, Y., Rohrbach, M., Yan, Z., Shuicheng, Y., Feng, J., Kalantidis, Y., 2019. Graph-based global reasoning networks. In: Proceedings of the IEEE/CVF Conference on Computer Vision and Pattern Recognition. pp. 433–442.
- Coalson, T.S., Van Essen, D.C., Glasser, M.F., 2018. The impact of traditional neuroimaging methods on the spatial localization of cortical areas. *Proc. Natl. Acad. Sci.* 115 (27), E6356–E6365.
- Cole, M.W., Ito, T., Bassett, D.S., Schultz, D.H., 2016. Activity flow over resting-state networks shapes cognitive task activations. *Nature Neurosci.* 19 (12), 1718–1726.
- De Benedictis, A., Duffau, H., Paradiso, B., Grandi, E., Balbi, S., Granieri, E., Colarutto, E., Chioffi, F., Marras, C.E., Sarubbo, S., 2014. Anatomofunctional study of the temporo-parieto-occipital region: dissection, tractographic and brain mapping evidence from a neurosurgical perspective. *J. Anatomy* 225 (2), 132–151.
- Deng, H., Birdal, T., Ilic, S., 2018. Ppfnet: Global context aware local features for robust 3d point matching. In: Proceedings of the IEEE Conference on Computer Vision and Pattern Recognition. pp. 195–205.
- Desikan, R.S., Ségonne, F., Fischl, B., Quinn, B.T., Dickerson, B.C., Blacker, D., Buckner, R.L., Dale, A.M., Maguire, R.P., Hyman, B.T., et al., 2006. An automated labeling system for subdividing the human cerebral cortex on MRI scans into gyral based regions of interest. *Neuroimage* 31 (3), 968–980.
- Destrieux, C., Fischl, B., Dale, A., Halgren, E., 2010. Automatic parcellation of human cortical gyri and sulci using standard anatomical nomenclature. *Neuroimage* 53 (1), 1–15.
- Dohmatob, E., Richard, H., Pinho, A.L., Thirion, B., 2021. Brain topography beyond parcellations: local gradients of functional maps. *NeuroImage* 229, 117706.
- Ellis, D.G., White, M.L., Hayasaka, S., Warren, D.E., Wilson, T.W., Aizenberg, M.R., 2020. Accuracy analysis of fMRI and MEG activations determined by intraoperative mapping. *Neurosurgical Focus* 48 (2), E13.
- Fernández, V., Llinás-Benadero, C., Borrell, V., 2016. Cerebral cortex expansion and folding: what have we learned? *EMBO J.* 35 (10), 1021–1044.
- Fey, M., Lenssen, J.E., Weichert, F., Müller, H., 2018. Splinecnn: Fast geometric deep learning with continuous b-spline kernels. In: Proceedings of the IEEE Conference on Computer Vision and Pattern Recognition. pp. 869–877.
- Finn, E.S., Shen, X., Scheinost, D., Rosenberg, M.D., Huang, J., Chun, M.M., Papademetris, X., Constable, R.T., 2015. Functional connectome fingerprinting: identifying individuals using patterns of brain connectivity. *Nature Neurosci.* 18 (11), 1664–1671.
- Fischl, B., 2012. FreeSurfer. *Neuroimage* 62 (2), 774–781.
- Gal, Y., Ghahramani, Z., 2016. Dropout as a bayesian approximation: Representing model uncertainty in deep learning. In: International Conference on Machine Learning. PMLR, pp. 1050–1059.
- Ge, L., Ren, Z., Yuan, J., 2018. Point-to-point regression pointnet for 3d hand pose estimation. In: Proceedings of the European Conference on Computer Vision. ECCV, pp. 475–491.
- Girshick, R., 2015. Fast r-cnn. In: Proceedings of the IEEE International Conference on Computer Vision. pp. 1440–1448.
- Glasser, M.F., Sotiropoulos, S.N., Wilson, J.A., Coalson, T.S., Fischl, B., Andersson, J.L., Xu, J., Jbabdi, S., Webster, M., Polimeni, J.R., et al., 2013. The minimal preprocessing pipelines for the human connectome project. *Neuroimage* 80, 105–124.
- Gopinath, K., Desrosiers, C., Lombaert, H., 2019. Graph convolutions on spectral embeddings for cortical surface parcellation. *Med. Image Anal.* 54, 297–305.
- Guedj, C., Vuilleumier, P., 2020. Functional connectivity fingerprints of the human pulvinar: Decoding its role in cognition. *NeuroImage* 221, 117162.

- He, W., Jiang, Z., Zhang, C., Sainju, A.M., 2020. Curvonet: Geometric deep learning based on directional curvature for 3d shape analysis. In: Proceedings of the 26th ACM SIGKDD International Conference on Knowledge Discovery & Data Mining. pp. 2214–2224.
- Huster, R.J., Westerhausen, R., Herrmann, C., 2011. Sex differences in cognitive control are associated with midcingulate and callosal morphology. *Brain Struct. Funct.* 215 (3), 225–235.
- Hutton, C., Josephs, O., Stadler, J., Featherstone, E., Reid, A., Speck, O., Bernarding, J., Weiskopf, N., 2011. The impact of physiological noise correction on fMRI at 7 T. *Neuroimage* 57 (1), 101–112.
- Im, K., Grant, P.E., 2019. Sulcal pits and patterns in developing human brains. *Neuroimage* 185, 881–890.
- Jiang, X., Zhang, T., Zhang, S., Kendrick, K.M., Liu, T., 2021. Fundamental functional differences between gyri and sulci: implications for brain function, cognition, and behavior. *Psychoradiology* 1 (1), 23–41.
- Ju, L., Wang, X., Wang, L., Mahapatra, D., Zhao, X., Zhou, Q., Liu, T., Ge, Z., 2022. Improving medical images classification with label noise using dual-uncertainty estimation. *IEEE Trans. Med. Imaging*.
- Kannurpatti, S.S., Biswal, B.B., 2012. Prediction of task-related BOLD fMRI with amplitude signatures of resting-state fMRI. *Front. Syst. Neurosci.* 6, 7.
- Kendall, A., Badrinarayanan, V., Cipolla, R., 2015. Bayesian segnet: Model uncertainty in deep convolutional encoder-decoder architectures for scene understanding. arXiv preprint arXiv:1511.02680.
- Kulason, S., Tward, D.J., Brown, T., Sicat, C.S., Liu, C.-F., Ratnanather, J.T., Younes, L., Bakker, A., Gallagher, M., Albert, M., et al., 2019. Cortical thickness atrophy in the transentorhinal cortex in mild cognitive impairment. *NeuroImage Clin.* 21, 101617.
- LeCun, Y., Bengio, Y., Hinton, G., 2015. Deep learning. *Nature* 521 (7553), 436–444.
- LeCun, Y., Bengio, Y., et al., 1995. Convolutional networks for images, speech, and time series. In: *The Handbook of Brain Theory and Neural Networks*, vol. 3361, no. 10. p. 1995.
- Li, Y., Sescousse, G., Amiez, C., Dreher, J.-C., 2015. Local morphology predicts functional organization of experienced value signals in the human orbitofrontal cortex. *J. Neurosci.* 35 (4), 1648–1658.
- Liu, T.T., 2016. Noise contributions to the fMRI signal: An overview. *NeuroImage* 143, 141–151.
- Liu, C., Frank, Q.Y., Newman, J.D., Szczupak, D., Tian, X., Yen, C.C.-C., Majka, P., Glen, D., Rosa, M.G., Leopold, D.A., et al., 2020. A resource for the detailed 3D mapping of white matter pathways in the marmoset brain. *Nature Neurosci.* 23 (2), 271–280.
- Long, K.R., Newland, B., Florio, M., Kalebic, N., Langen, B., Kolterer, A., Wimberger, P., Huttner, W.B., 2018. Extracellular matrix components HAPLN1, lumican, and collagen I cause hyaluronic acid-dependent folding of the developing human neocortex. *Neuron* 99 (4), 702–719.
- Lopez-Persem, A., Verhagen, L., Amiez, C., Petrides, M., Sallet, J., 2019. The human ventromedial prefrontal cortex: sulcal morphology and its influence on functional organization. *J. Neurosci.* 39 (19), 3627–3639.
- Monti, F., Boscaini, D., Masci, J., Rodola, E., Svoboda, J., Bronstein, M.M., 2017. Geometric deep learning on graphs and manifolds using mixture model cnns. In: *Proceedings of the IEEE Conference on Computer Vision and Pattern Recognition*. pp. 5115–5124.
- Ngo, G.H., Khosla, M., Jamison, K., Kuceyeski, A., Sabuncu, M.R., 2022. Predicting individual task contrasts from resting-state functional connectivity using a surface-based convolutional network. *NeuroImage* 248, 118849.
- Nguyen, D.-P., Tho, M.-C.H.B., Dao, T.-T., 2021. Enhanced facial expression recognition using 3D point sets and geometric deep learning. *Med. Biol. Eng. Comput.* 1–10.
- Papo, D., 2019. Gauging functional brain activity: from distinguishability to accessibility. *Front. Physiol.* 10, 509.
- Qi, C.R., Su, H., Mo, K., Guibas, L.J., 2017a. Pointnet: Deep learning on point sets for 3d classification and segmentation. In: *Proceedings of the IEEE Conference on Computer Vision and Pattern Recognition*. pp. 652–660.
- Qi, C.R., Yi, L., Su, H., Guibas, L.J., 2017b. Pointnet++: Deep hierarchical feature learning on point sets in a metric space. arXiv preprint arXiv:1706.02413.
- Reardon, P., Seidlitz, J., Vandekar, S., Liu, S., Patel, R., Park, M.T.M., Alexander-Bloch, A., Clasen, L.S., Blumenthal, J.D., Lalonde, F.M., et al., 2018. Normative brain size variation and brain shape diversity in humans. *Science* 360 (6394), 1222–1227.
- Ribeiro, F., Bollmann, S., Puckett, A., 2021. Predicting the retinotopic organization of human visual cortex from anatomy using geometric deep learning. *NeuroImage* 244, 118624.
- Schultz, R.T., Cho, N.K., Staib, L.H., Kier, L.E., Fletcher, J.M., Shaywitz, S.E., Shankweiler, D.P., Katz, L., Gore, J.C., Duncan, J.S., et al., 1994. Brain morphology in normal and dyslexic children: The influence of sex and age. *Ann. Neurol.* 35 (6), 732–742.
- Shrout, P.E., Fleiss, J.L., 1979. Intraclass correlations: uses in assessing rater reliability. *Psychol. Bull.* 86 (2), 420.
- Simpson, S.L., Moussa, M.N., Laurienti, P.J., 2012. An exponential random graph modeling approach to creating group-based representative whole-brain connectivity networks. *NeuroImage* 60 (2), 1117–1126.
- Srivastava, N., Hinton, G., Krizhevsky, A., Sutskever, I., Salakhutdinov, R., 2014. Dropout: a simple way to prevent neural networks from overfitting. *J. Mach. Learn. Res.* 15 (1), 1929–1958.
- Suárez, L.E., Markello, R.D., Betzel, R.F., Misic, B., 2020. Linking structure and function in macroscale brain networks. *Trends Cognit. Sci.* 24 (4), 302–315.
- Sun, Z., Pinel, P., Rivière, D., Moreno, A., Dehaene, S., Mangin, J.-F., 2016. Linking morphological and functional variability in hand movement and silent reading. *Brain Struct. Funct.* 221 (7), 3361–3371.
- Tavor, I., Jones, O.P., Mars, R.B., Smith, S., Behrens, T., Jbabdi, S., 2016. Task-free MRI predicts individual differences in brain activity during task performance. *Science* 352 (6282), 216–220.
- Thompson, P., Schwartz, C., Toga, A., 1996. High-resolution random mesh algorithms for creating a probabilistic 3D surface atlas of the human brain. *NeuroImage* 3 (1), 19–34.
- Troiani, V., Patti, M.A., Adamson, K., 2020. The use of the orbitofrontal H-sulcus as a reference frame for value signals. *Eur. J. Neurosci.* 51 (9), 1928–1943.
- Van Essen, D.C., Smith, S.M., Barch, D.M., Behrens, T.E., Yacoub, E., Ugurbil, K., Consortium, W.-M.H., et al., 2013. The WU-minn human connectome project: an overview. *NeuroImage* 80, 62–79.
- Van Essen, D.C., Ugurbil, K., Auerbach, E., Barch, D., Behrens, T.E., Bucholz, R., Chang, A., Chen, L., Corbetta, M., Curtiss, S.W., et al., 2012. The human connectome project: a data acquisition perspective. *NeuroImage* 62 (4), 2222–2231.
- Van Tol, M.-J., Li, M., Metzger, C., Hailla, N., Horn, D., Li, W., Heinze, H., Bogerts, B., Steiner, J., He, H., et al., 2014. Local cortical thinning links to resting-state disconnectivity in major depressive disorder. *Psychol. Med.* 44 (10), 2053–2065.
- Veličković, P., Cucurull, G., Casanova, A., Romero, A., Lio, P., Bengio, Y., 2017. Graph attention networks. arXiv preprint arXiv:1710.10903.
- Verma, N., Boyer, E., Verbeek, J., 2018. Feastnet: Feature-steered graph convolutions for 3d shape analysis. In: *Proceedings of the IEEE Conference on Computer Vision and Pattern Recognition*. pp. 2598–2606.
- Wang, L., Huang, Y., Hou, Y., Zhang, S., Shan, J., 2019a. Graph attention convolution for point cloud semantic segmentation. In: *Proceedings of the IEEE/CVF Conference on Computer Vision and Pattern Recognition*. pp. 10296–10305.
- Wang, Y., Sun, Y., Liu, Z., Sarma, S.E., Bronstein, M.M., Solomon, J.M., 2019b. Dynamic graph cnn for learning on point clouds. *AcM Trans. Graphics (Tog)* 38 (5), 1–12.
- Welling, M., Kipf, T.N., 2017. Semi-supervised classification with graph convolutional networks. In: *J. International Conference on Learning Representations (ICLR 2017)*.
- Whittle, S., Allen, N.B., Fornito, A., Lubman, D.I., Simmons, J.G., Pantelis, C., Yücel, M., 2009. Variations in cortical folding patterns are related to individual differences in temperament. *Psychiatry Res. Neuroimaging* 172 (1), 68–74.
- Willerman, L., Schultz, R., Rutledge, J.N., Bigler, E.D., 1991. In vivo brain size and intelligence. *Intelligence* 15 (2), 223–228.
- Woo, S., Park, J., Lee, J.-Y., Kweon, I.S., 2018. Cbam: Convolutional block attention module. In: *Proceedings of the European Conference on Computer Vision. ECCV*, pp. 3–19.
- Wu, Z., Pan, S., Chen, F., Long, G., Zhang, C., Philip, S.Y., 2020. A comprehensive survey on graph neural networks. *IEEE Trans. Neural Netw. Learn. Syst.* 32 (1), 4–24.
- Zamboni, G., Wilcock, G.K., Douaud, G., Drazich, E., McCulloch, E., Filippini, N., Tracey, I., Brooks, J.C., Smith, S.M., Jenkinson, M., et al., 2013. Resting functional connectivity reveals residual functional activity in Alzheimer's disease. *Biol. Psychiat.* 74 (5), 375–383.
- Zhang, K., Sejnowski, T.J., 2000. A universal scaling law between gray matter and white matter of cerebral cortex. *Proc. Natl. Acad. Sci.* 97 (10), 5621–5626.
- Zhang, Y., Zhou, Y., Yu, C., Lin, L., Li, C., Jiang, T., 2010. Reduced cortical folding in mental retardation. *Am. J. Neuroradiol.* 31 (6), 1063–1067.
- Zhao, H., Jiang, L., Jia, J., Torr, P.H., Koltun, V., 2021. Point transformer. In: *Proceedings of the IEEE/CVF International Conference on Computer Vision*. pp. 16259–16268.
- Zhao, F., Xia, S., Wu, Z., Duan, D., Wang, L., Lin, W., Gilmore, J.H., Shen, D., Li, G., 2019. Spherical U-Net on cortical surfaces: methods and applications. In: *International Conference on Information Processing in Medical Imaging*. Springer, pp. 855–866.
- Zheng, Z., Yang, Y., 2021. Rectifying pseudo label learning via uncertainty estimation for domain adaptive semantic segmentation. *Int. J. Comput. Vis.* 129 (4), 1106–1120.
- Zuo, X.-N., Di Martino, A., Kelly, C., Shehzad, Z.E., Gee, D.G., Klein, D.F., Castellanos, F.X., Biswal, B.B., Milham, M.P., 2010. The oscillating brain: complex and reliable. *NeuroImage* 49 (2), 1432–1445.